PI and Adaptive Model Matching Control System that Satisfies the Setting Settling Time application to engine speed control

Takeshi Takiyama * **Tatsuya Yoshikawa** ** **Jinto Noh** ** **Yuzo Ohta** ***

* *Osaka City University, Osaka, Japan,*
(e-mail: takiyama@mech.eng.osaka-cu.ac.jp)
** *Osaka City University, Graduate school, Osaka, Japan*
*** *Kobe University, Kobe, Japan*

Abstract: A new design method that satisfies the setting settling time with small maximum overshoot in a servo controller was developed using a PI controller and an internal feedback system. The internal feedback system consists of the model parameter of the controlled object that was approximated as a second-order lag-time system. Therefore, an adaptive ability that counteracts the changing model parameters was required. In this paper, the variable parameters of the controlled object were obtained by on-line execution of a non-linear least-squares method. Suitable adaptation by the developed method was confirmed in simulation and experimental tests.

Keywords: Engine Control, Adaptive Control, Settling Time, PI Control, Model Matching, Non-linear Least-Squares Sequential Quadratic Programming

1. INTRODUCTION

In order to reduce the CO2 emission of an automobile, an optimal control is necessary to operate the power train with high efficiency. Then, since the parameters of a dynamic characteristics of the power train vary according to the driving condition, non-linear compensation is required for the control system [Takiyama (2014)]. Besides, since the number of power train component is increased for high efficient operation, it is desirable that the control system can be easily and conveniently constructed for an efficient development.

PID controllers are widely used for closed-loop systems from the viewpoints of simplicity and control performance. Though various methods are considered to determine the control parameters [Ålström and Hägglund (1995)], those are obtained by evaluating the settling time or overshoot of the time response in numerous trial-and-error cases. A coefficient diagram method that consider both the dynamics of the target system and the time response were proposed [Manabe (1998)], however, it is complicated. And, the dead-beat controller is a well-known controller that satisfies the setting settling time, but lacks robustness. Recently, a method for optimizing the control parameters using a non-linear programming method has been proposed based on the measured input/output data to/from the controlled object [Kaneko (2013)]. Therefore, the non-linear programming method is expected to obtain a suitable parameter of the dynamic characteristics of the controlled object.

In a normal second-order lag-time system, the time response is known to depend on the damping coefficient or frequency parameter. Based on this background, we investigate a new design method of a servo system that satisfies the setting settling time with small overshoot amount without trial-and-error. The controller consists of a proportional integral (PI) controller and an internal controller for a second-order lag-time system using the model parameters of the control objects [Ohta, et al. (2014)]. Since the control system can be simply constructed by using the desired settling time, it is very useful to improve the efficient development of control system. Furthermore, changes in the parameters of the controlled object are handled by an adaptation method implemented in the control system by an on-line parameter search using a non-linear programming method.

This paper investigated about PI and adaptive model matching control system that satisfies the setting settling time. Then, it was applied to the speed controller of a gasoline engine and the experimental examination were carried out.

2. SETTING SETTLING TIME SERVO SYSTEM

2.1 PI Controller and Settling Time in the Second-order Lag-time System

Figure 1 shows the unity feedback system. In (1) and (2) respectively, $P(s)$ denotes a virtual control object in the second-order lag-time system and $C_{PI}(s)$ denotes the PI controller. Equation (3) defines the M% overshoot. The smallest T_s that satisfies (3), called the M% settling time, is denoted as $T_s(M)$.

$$P(s) = \frac{{\omega_n}^2}{s^2 + 2\zeta\omega_n s + {\omega_n}^2} \tag{1}$$

$$C_{PI}(s) = K_P + K_I \frac{1}{s} \tag{2}$$

$$\frac{|y(t) - y(\infty)|}{|y(\infty)|} \times 100 \leqq M, \ t \geqq T_s \tag{3}$$

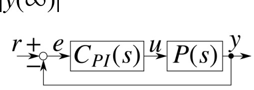

Fig. 1. Unity feedback system

The step-response characteristics of this closed loop system were investigated in numerical experiments. In these experiments, we select ω_n=10, $M\in\{1, 2, 5, 10\}$, $\zeta\in\{0.3, 0.4, 0.5, 0.6, 0.7, 0.8, 0.9, 1.0, 1.1\}$ and $K_P \in\{0.01, 0.02,\cdots, 10.00\}$. Then, we investigated the K_I value that stabilized the closed loop and minimized $T_s(M)$ for different combinations of (M, ζ, K_P) triples. Then, in order to diminish the maximum overshoot less than $M\%$, ζ was investigated that achieve a small T_s at a relatively low gain crossover frequency ω_g. Ultimately, we selected ζ= 0.7 for M=2. The experimental results as M was varied from 1 to 10 are presented in Table 1 [Ohta, et al. (2014)].

Table 1. Recommended value of ζ, K_P, K_I and corresponding values of $T_s(M)$, phase margin ϕ_m, and ω_g for each $M\{1, 2, 5, 10\}$, where ω_n=10

M	ζ	K_P	K_I	$T_s(M)$	ϕ_m	ω_g
1	0.7	0.11	3.44	0.597	67.6	3.44
2	0.7	0.28	4.39	0.442	67.7	4.49
5	0.6	0.27	4.77	0.356	66.0	5.18
10	0.6	0.71	6.88	0.223	55.5	8.64

2.2 Control System that Satisfies the Setting Settling Time

For example, when ω_n=10 and a 2% settling time $\widehat{T_s}$ is required, the controller parameters can be read from Table 1: ζ=0.7, K_P=0.28, K_I=4.39 and $T_s(2)$=0.442 for M=2. According to the similarity theorem of the Laplace transform, the $M\%$ settling time $T_s(M)$ and the setting settling time $\widehat{T_s}$ are related through α (see (4)) [Ohta, et al. (2014)]. Applying the PI controller of (6) to the system governed by (5), the 2% settling time of the step response of the closed-loop transfer function ($G_r(s)$ in (7)) satisfies the $\widehat{T_s}$. Hereafter, we refer to $G_r(s)$ as the reference model (where the subscript r denotes reference).

$$\alpha = \frac{T_s(M)}{\widehat{T_s}} = \frac{T_s(2)}{\widehat{T_s}} = \frac{0.442}{\widehat{T_s}}, \quad \omega_n = 10 \tag{4}$$

$$P_r(s) = \frac{(\alpha\omega_n)^2}{s^2+2\zeta(\alpha\omega_n)s+(\alpha\omega_n)^2} = \frac{(\alpha\omega_n)^2}{D(s)} \tag{5}$$

$$C_{PI}(s) = K_P + \frac{\alpha K_I}{s} = 0.28 + \frac{\alpha 4.39}{s} \tag{6}$$

$$G_r(s) = \frac{C_{PI}(s)P_r(s)}{1 + C_{PI}(s)P_r(s)} \tag{7}$$

2.3 Servo System using Internal Feedback

Equation (8) describes a general second-order lag-time system $P_f(s)$. A servo system that satisfies the setting $M\%$ settling time $\widehat{T_s}(M)$ was constructed using an internal feedback controller. The internal feedback controller was constructed following the pole-assignment method with a dynamic controller using a minimum-order observer [Ichikawa (1985)]. Figure 2 shows the structure of the system. The transfer function $\widehat{P_f}(s)$ from u_a to y, given by (9), depends on the gain K_a and the internal feedbacks $C_{bu}(s)$ and $C_{by}(s)$.

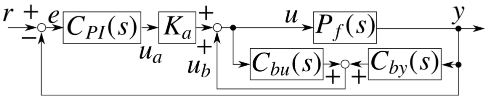

Fig. 2. Structure of the control system

$$P_f(s) = \frac{b_0}{s^2 + a_1 s + a_0} \tag{8}$$

$$\widehat{P_f}(s) = \frac{Y(s)}{U_a(s)} = \frac{K_a P_f(s)}{1+C_{bu}(s)+P_f(s)C_{by}(s)} \tag{9}$$

$$K_a = \frac{(\alpha\omega_n)^2}{b_0}, C_{bu}(s) = \frac{q-\gamma}{s+\gamma}, C_{by}(s) = \frac{r_1 s+r_0}{b_0(s+\gamma)} \tag{10}$$

$$q = 2\zeta(\alpha\omega_n) + \gamma - a_1 \tag{11}$$

$$r_1 = (\alpha\omega_n)^2 + 2\zeta\gamma(\alpha\omega_n) - a_1 q - a_0 \tag{12}$$

$$r_0 = \gamma(\alpha\omega_n)^2 - a_0 q \tag{13}$$

$$\widehat{P_f}(s) = \frac{K_a P_f(s)}{1+C_{bu}(s)+P_f(s)C_{by}(s)} = \frac{(s+\gamma)K_a b_0}{(s+\gamma)D(s)} = P_r(s) \tag{14}$$

$$G_f(s) = \frac{C_{PI}(s)\widehat{P_f}(s)}{1+C_{PI}(s)\widehat{P_f}(s)} = \frac{(s+\gamma)C_{PI}(s)P_r(s)}{(s+\gamma)[1+C_{PI}(s)P_r(s)]} = G_r(s) \tag{15}$$

Using the parameters described in (10)-(13), $\widehat{P_f}(s)$ equals $P_r(s)$ and the closed-loop transfer function $G_f(s)$ equals $G_r(s)$. These relationships are described by (14) and (15), respectively. Therefore, the general second-order lag-time system with the internal feedback match the reference model and the system can satisfy the setting settling time. The control system that satisfies the $M\%$ settling time $\widehat{T_s}$ is called the setting settling time controller (SSTC) hereafter. Note that the denominator and numerator of (14) and (15) are offset by (s+γ), where $-\gamma$ denotes the pole of the minimum-order observer. To preserve the responsiveness of the system, the value of γ should be sufficiently larger than the other poles and zeros of $G_f(s)$ (for example, five times or higher).

3. NON-LINEAR PROGRAMMING

The model parameters of the controlled object vary under several influences. This variation must be corrected by some kind of countermeasure for the SSTC. In this paper, a changing parameter is detected from variations in the dynamic characteristics of the transient response. The calculation is performed by non-linear least squares sequential quadratic programming (NLSSQP). The NLSSQP method combines the quasi-Newton method for the unconstrained non-linear least-squares problem with the SQP method for general non-linear minimization problems [Takahashi (1987)]. The objective is to determine the $\boldsymbol{x}$ that minimizes the objective function (18) under the constraints described by (16) and (17). In (18), $\boldsymbol{r}(\boldsymbol{x})$ stands for the residual vector.

$$\boldsymbol{g}(\boldsymbol{x}) \leqq \boldsymbol{0}, \boldsymbol{g}(\boldsymbol{x}) = [g_1(\boldsymbol{x}), \cdots, g_m(\boldsymbol{x})]^T \tag{16}$$

$$\boldsymbol{h}(\boldsymbol{x}) = \boldsymbol{0}, \boldsymbol{h}(\boldsymbol{x}) = [h_1(\boldsymbol{x}), \cdots, h_l(\boldsymbol{x})]^T \tag{17}$$

$$f(x) = \frac{1}{2}\boldsymbol{r}(\boldsymbol{x})^T\boldsymbol{r}(\boldsymbol{x}) = \frac{1}{2}\sum_{j=1}^{p}\left[\boldsymbol{r}_j(\boldsymbol{x})\right]^2 \tag{18}$$

This problem was solved by a sequential quadratic-programming algorithm. Given $\boldsymbol{x}_k$, this partial QP problem seeks the $\boldsymbol{d} \in R^n$ that minimizes (21) under the linear constraint conditions described by (19) and (20). Figure 3 is a flow-chart of the NLSSQP method. The direction $\boldsymbol{d}$ was searched by the Goldfarb-Idnani method, and the minimum step size β was determined by a golden sectioning method.

$$\boldsymbol{g}(\boldsymbol{x}_k) + \nabla \boldsymbol{g}(\boldsymbol{x}_k)\boldsymbol{d} \leqq 0 \tag{19}$$

$$\boldsymbol{h}(\boldsymbol{x}_k) + \nabla \boldsymbol{h}(\boldsymbol{x}_k)\boldsymbol{d} = 0 \tag{20}$$

$$\operatorname{argmin}\left[\frac{1}{2}\boldsymbol{d}^T \boldsymbol{B}_k \boldsymbol{d} + \boldsymbol{r}(\boldsymbol{x}_k)^T \boldsymbol{J}(\boldsymbol{x}_k)\boldsymbol{d}\right], \boldsymbol{d} \in R^n \tag{21}$$

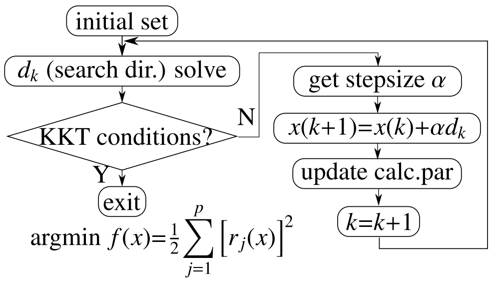

Fig. 3. Flow-chart of NLSSQP

4. CONTROL SYSTEM

4.1 Experimental Apparatus and Objective System

The experiments were performed on a gasoline engine installed on a test-bench without an equivalent inertial mass. The engine has three cylinders and a displacement of 660cc. It was controlled by a digital signal processing (mtt iBIS(DSP7101)). The measurement and control were executed at every suction action of the top dead center of cylinder #1. Therefore, the sampling-and-control time Δt was set to $\Delta t=2/n_e$, where n_e represents the engine speed (s^{-1}).

The target was the engine speed n_e, controlled by commanding the ignition timing I_g. The objective model (see Fig. 4) was based on on our previous investigation and the step response shown in Fig. 6. The transfer function is given by (22), and the operating conditions are shown in Fig. 5. The intake valve opening (IVO) angle was set to 0 or 20 CA (where CA denotes

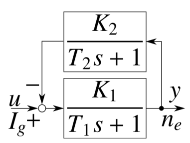

Fig. 4. Objective model of the target system

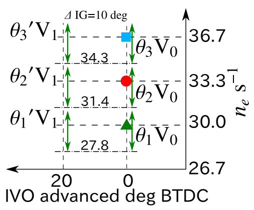

Fig. 5. Operating points for model identification

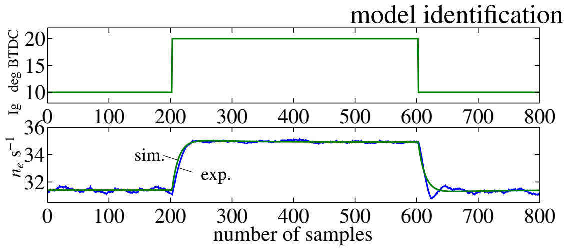

Fig. 6. Model identification results (at θ_2'V$_1$)

Table 2. Identified model parameter

IVO adv.	20	0	20	0	20	0
	θ_3'V$_1$	θ_3V$_0$	θ_2'V$_1$	θ_2V$_0$	θ_1'V$_1$	θ_1V$_0$
T_1	0.7	0.9	0.65	0.75	0.7	0.8
K_1	0.42	0.39	0.37	0.37	0.35	0.33
T_2	5.0	5.0	5.0	5.0	5.0	5.0
K_2	0.11	0.15	0.14	0.24	0.13	0.18

the crank angle). Figure 6 shows a typical identification result. The upper and lower panels display the time responses of the ignition timing I_g and the engine speed n_e, respectively. During the step-down of the I_g, the time responses of the objective model (sim.) and experimental results (exp.) slightly deviated because parameters such as the time constant of the intake system differ at deceleration and acceleration. Otherwise, the model output well agreed with the engine output, verifying the suitability of this objective model as a controller design. Table 2 provides the identified model parameters under each operating condition. Although the engine speed varied within 10 s^{-1}, the time constant T_1 and gain K_1 varied by 20-30%. These parameters were then targeted for adaptation.

$$P_{p_0}(s) = \frac{N_E(s)}{I_G(s)} = \frac{\frac{K_1}{T_1 T_2}(T_2 s + 1)}{s^2 + \frac{T_1+T_2}{T_1 T_2}s + \frac{1+K_1 K_2}{T_1 T_2}} \tag{22}$$

4.2 Construction of SSTC for Speed Controller

The relative order of the transfer function of the controlled objective $P_{p_0}(s)$ (22) is a first-order. To translate the second-order system, a compensator $C_p(s)$ was connected in series with (22). Equation (23) denotes the second-order lag-time system after compensation. Substituting the parameters a_1, a_0, and b_0 (defined by (24)) into (10)-(13), we construct the control system shown in Fig. 7. In this way, we can automatically construct the SSTC based on the correct model parameters and the setting settling time.

$$P_f(s)=C_p(s)P_{p_0}(s)=\frac{\frac{K_1}{T_1 T_2}}{s^2+\frac{T_1+T_2}{T_1 T_2}s+\frac{1+K_1 K_2}{T_1 T_2}}, C_p(s)=\frac{1}{T_2 s+1} \tag{23}$$

$$a_1 = \frac{T_1 + T_2}{T_1 T_2}, a_0 = \frac{1 + K_1 K_2}{T_1 T_2}, b_0 = \frac{K_1}{T_1 T_2} \tag{24}$$

$$\zeta = 0.7,\ \omega_n = 10,\ \gamma = 10 \tag{25}$$

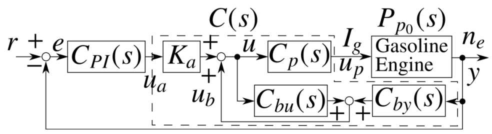

Fig. 7. Structure of the engine control system

4.3 Construction of Real-Time Adaptive Control System

Figure 8 schematizes the adaptive control system with SSTC. The $P_p(s)$ in Fig. 8 represents a virtual model with the same structure as the engine model $P_{p_0}(s)$. The $C(s)$ represents the overall control system comprising the SSTC's internal feedback control system ($K_a, C_{bu}(s), C_{by}(s)$ described by (10)) and the compensator $C_p(s)$. These compartments are delined by the dashed line in Fig. 7. The parameter value of $C(s)$ was set equal to that of $P_p(s)$.

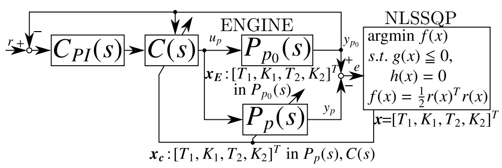

Fig. 8. Schematic of the adaptive control system

The feedback control to the controlled object $P_{p_0}(s)$ was performed through the output y_{p_0}. To obtain the open-loop response y_p, the u_p control signal was commanded to the $P_p(s)$ at the same time. As the virtual model $P_p(s)$ and the controlled object model $P_{p_0}(s)$ are structurally identical and the same input is commanded, the parameter difference is expected to be detectable from the output difference.

4.4 Procedure of On-line Real-time NLSSQP Operation

Figure 9 displays the procedure of the on-line real-time NLSSQP. Note that the model parameters $[T_1, K_1, T_2, K_2]$ in the controlled object $P_{p_0}(s)$ are expressed in vector form as $\boldsymbol{x}_E$ (where the subscript E denotes engine), and those in the virtual model $P_p(s)$ and the SSTC $C(s)$ are expressed as $\boldsymbol{x}_C$ (where the subscript C denotes controller).

While $1 \leqq k \leqq 150$, the first procedure (indicated by (s)) stores the input u_p and the output y_{p_0} of the controlled object. The following procedure (a) calculates the open response of $P_p(s)$ using u_p, (b) sets the residual vector, and (c) executes NLSSQP to obtain $\boldsymbol{x}_C$. Finally, it (d) updates $P_p(s)$ and $C(s)$ using $\boldsymbol{x}_C$. Routines (a)-(d) are iterated for $151 \leqq k \leqq 250$. When $\widetilde{n}_e$ changes, the procedure returns to (s) and the adaptation repeats.

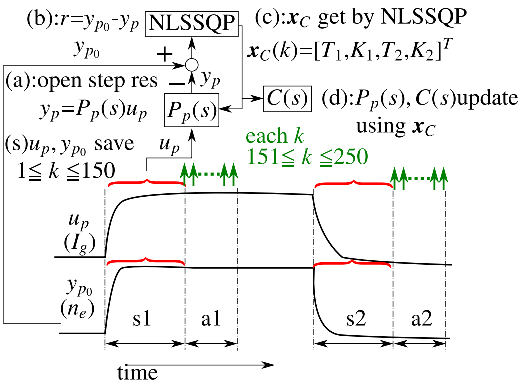

Fig. 9. Schematic of on-line NLSSQP

4.5 Constraint Conditions

Equations (26)-(27) are assigned as constraint conditions to accelerate convergence of the parameter exploration. Equation (26) restricts the range of each parameter. Based on the identification results in Table 2, these ranges were determined as 20% above the maximum and 20% below the minimum value.

$$0.45 \leqq T_1 \leqq 1.1,\ 0.21 \leqq K_1 \leqq 0.51,\ 4 \leqq T_2 \leqq 6,\ 0.05 \leqq K_2 \leqq 0.29 \quad (26)$$

$$g_1 = j_1 T_1 + j_2 K_1 + j_3 T_2 + j_4 K_2 \leqq 0 \quad (27)$$

For every change in T_1 and K_1, T_2 and K_2 were changed through (27). Investigation showed that the convergence speed and accuracy of matching $\boldsymbol{x}_C$ and $\boldsymbol{x}_E$ depend on the values of the coefficients j_1-j_4 in (27). Figure 10 plots the concordance rate $\boldsymbol{x}_C/\boldsymbol{x}_E$ for each combination p_1-p_5 of j_1-j_4 listed in Table 3. When the concordance rate approximates 1, $\boldsymbol{x}_C$ and $\boldsymbol{x}_E$ are well-matched. Based on these results, we selected the p_2 combination with j_1=-1, j_2=-1, j_3=0.2 and j_4=0.1.

Table 3. INEQ par. combination

	j_1	j_2	j_3	j_4
p_1	-1	-1	0.3	0.1
p_2	-1	-1	0.2	0.1
p_3	-1	-1	0.1	0.1
p_4	-1	-1	0.2	0.2
p_5	-1	-1	0.2	0.01

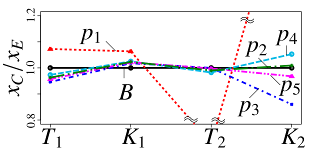

Fig. 10. Concordance rate for each combination p_n of INEQ coefficients

5. SIMULATION AND EXPERIMENTATION

To clarify the adaptation process, the dynamic behavior of the controller was set slower than that of the controlled object. To this end, the parameter at θ_3V$_0$ with the largest time constant T_1 was applied to $\boldsymbol{x}_C$, while the parameter at θ_2'V$_1$ with the smallest T_1 was applied to $\boldsymbol{x}_E$. The $C(s)$ was designed with a 2% settling time $\widehat{T_s}(2)$=3s, and α was multiplied by 1.01 to provide a margin. As mentioned at 4.1, Δt=2/n_e ≈0.06(s).

Figure 11 illustrates the simulation results. The target engine speed ($\widetilde{n}_e$) was periodically increased and decreased. Figure 11(A) illustrates the time responses of the input and output signals of the controlled object. The upper panel presents the input $I_g(u_p)$, and the lower panel plots the $\widetilde{n}_e$ and output n_e. The n_e and $\widetilde{n}_e$ values are consistent, confirming a well-controlled output. Figure 11(A) also shows the input and output behavior of the reference model $G_r(s)$, represented by u_r and y_r respectively.

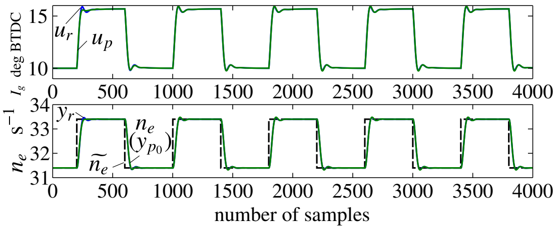

(A). Time responses of inputs and outputs

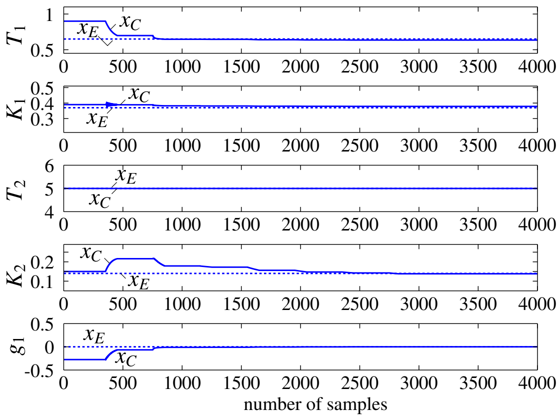

(B). Inequality constraints

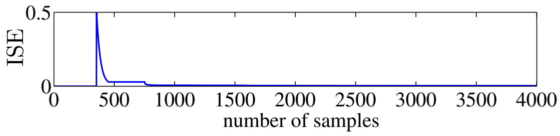

(C). Integrated square errors

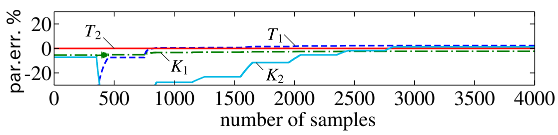

(D). Coincidence ratios of model parameters

Fig. 11. Results of the simulated adaptive control

As $n_e(y_{p_0})$ and y_r almost overlap after the second period of the $\widetilde{n_e}$ change, the NLSSQP is deemed effective.

Figure 11(B) illustrates the time response of each parameter of $\boldsymbol{x}_C$. The same time responses are elicited by the inequality constraints and by g_1 in (27). The range of the vertical axis covers the range of inequality constraints, confirming that each inequality constraint is satisfied. The dotted line in each panel plots the $\boldsymbol{x}_E$. At every $\widetilde{n_e}$ change, the parameter $\boldsymbol{x}_C$ at the controller side gradually changed over steps $151 \leqq k \leqq 250$ in one period, as mentioned above. In the third period of $\widetilde{n_e}$ change, the $\boldsymbol{x}_C$ almost coincided with the parameter $\boldsymbol{x}_E$ of the controlled object. This implies successful adaptive operation by NLSSQP. The integrated square error (ISE) (Fig. 11(C)) behaved similarly to the objective function of NLSSQP. During one period, ISE decreased throughout $151 \leqq k \leqq 250$ with every iteration of $\widetilde{n_e}$ change. Almost the same behavior occurred during an $\boldsymbol{x}_C$ change. Figure 11(D) illustrates the error ratio between the obtained parameter $\boldsymbol{x}_C$ and the controlled object parameter $\boldsymbol{x}_E$. The small residual was attributed to the limit of the parameter search when ISE became very small.

5.1 Consideration of Adaptive Behavior

To clarify the adaptive action during one period of $\widetilde{n_e}$ change, Fig. 12 superposes the adaptive behaviors at the first (k=151), fiftieth (k=200) and hundredth (k=250) instances in the first period of a $\widetilde{n_e}$ change. The upper panels of Fig. 12 depict y_{p_0} and $y_p(\boldsymbol{x}_C(k), l)$. The y_{p_0} is the stored data used in the NLSSQP processing, so remains constant throughout the period. The $y_p(\boldsymbol{x}_C(k), l)$ was obtained from the open response of $P_p(s)$ and supplied to the NLSSQP calculation at every k. During the $\widetilde{n_e}$ step-up in the first period of a $\widetilde{n_e}$ change, the virtual model output y_p(1st) and the controlled object output y_{p_0} were mismatched because the value of $\boldsymbol{x}_C$ at the controller side deviated from that of $\boldsymbol{x}_E$ at the controlled (object) side. Furthermore, y_{p_0} did not satisfy the setting $M\%$ settling time because the SSTC's parameters were designed using $\boldsymbol{x}_C$. However, between 50 and 100 steps, the the y_p gradually edged closer to y_{p_0}. The bottom panels of Fig. 12(A) plot the the squared error

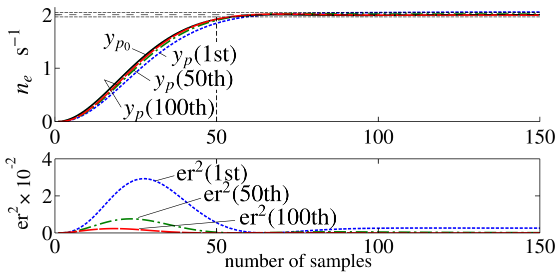

(A). during $\widetilde{n_e}$ step-up in the 1st period.

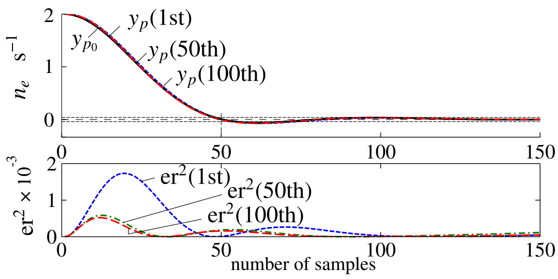

(B). during $\widetilde{n_e}$ step-down in the 1st period.

Fig. 12. Adaptive behavior using NLSSQP

$\mathrm{er}^2(l) = \left[y_{p_0}(l) - y_p(l)\right]^2$ at first, fiftieth and hundredth. During the $\widetilde{n_e}$ step-up, the error er^2 gradually decreased, demonstrating strong convergence of y_p to y_{p_0}. During a $\widetilde{n_e}$ step-down in the first period of a $\widetilde{n_e}$ change, y_p appears to reasonably agree with y_{p_0} (Fig. 12(B), top), but er^2 was not complementary attenuated (Fig. 12(B), bottom). The er^2 shown in Fig. 12(B) bottom had decreased to 1/10 of those in Fig. 12(A) bottom. Then, the difference of er^2 at 50 steps and at 100 steps is small. Therefore, the er^2 was to be sufficiently decreased and the adaptation was considered to be almost accomplished.

5.2 Consideration of Settling Time

Figure 13 illustrates the amplified y_{p_0} (n_e) behavior of the transient response in five periods of $\widetilde{n_e}$ change for $\widehat{T_s}(2)$=3 and 4s. The upper and lower panels present the responses during a $\widetilde{n_e}$ step-up and $\widetilde{n_e}$ step-down, respectively. The time response of y_r of reference model $G_r(s)$ is clarified by the × symbols in Fig. 13. Since y_r satisfies the setting settling time, the response through the × symbols also demonstrates satisfying the setting settling time. The indices s1-s10 indicate when the $\widetilde{n_e}$ changed. Odd and even indices denote a $\widetilde{n_e}$ step-up and a $\widetilde{n_e}$ step-down period, respectively. During the first period, the y_{p_0}(s1) (blue line) did not pass over the ×. However, the y_{p_0}(s3-s9) passed over and almost overlapped the × points. This confirms that the time responses of y_{p_0} satisfies the setting $M\%$ settling time $\widehat{T_s}(M)$. In the $\widetilde{n_e}$ step-down period (Fig. 13, lower), all behaviors almost passed over the × points, demonstrating near coincided of the time responses of y_{p_0} and y_r. Therefore, the setting $M\%$ settling time $\widehat{T_s}(M)$ was well satisfied in this case. The adaptation method almost accomplished until the second period of the $\widetilde{n_e}$ change and satisfied the setting settling times $\widehat{T_s}(2)$=3 and 4s, although some parameter deviations remained.

These results also demonstrate that the maximum overshoot becomes less than $M\%$.

5.3 Experimental Results

The physical experiments were carried out under similar conditions to the simulation study. The results are shown in Fig. 14. On average, the time responses of the input I_g and output n_e (Fig. 14(A)) reasonably agreed with those of $\widetilde{n_e}$. The fluctuation of n_e near $\widetilde{n_e}$ are attributable to combustion variations. The behavior of the reference model (u_r and y_r) is also depicted in the

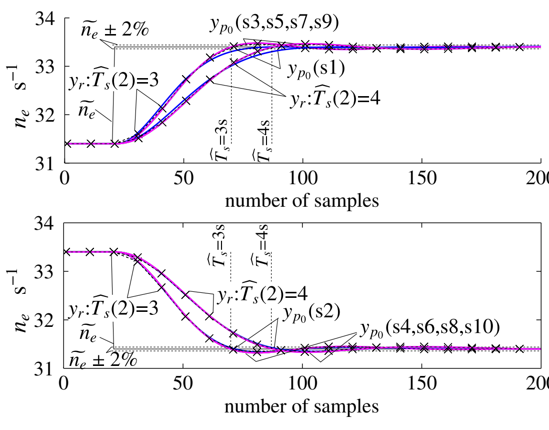

Fig. 13. Amplified transient response showing convergence to the settling time and adaptive behavior

figure. I_g(exp.) deviated from u_r because the engine parameters varied with the environmental conditions. This difference is especially noticeable during the third period. The largish variation in the engine parameters was probably caused by changes in factor such as combustion. Figure 14(B) illustrates the time responses of the parameters and the inequality constraint condition. Although it settled within the constraint range, $\boldsymbol{x}_C$ varied widely at each $\widetilde{n_e}$ change. T_1 and K_2 especially varied at the $\widetilde{n_e}$ step-down in the third period and the $\widetilde{n_e}$ step-up in the fourth period (indicated by arrows (→) in the figure). These changes were caused by the unfavorable work output of NLSSQP when the inputs-outputs relationship were deteriorated by the combustion variation in the third period, as mentioned above. Figure 14(C) illustrates the time response of the ISE. Again, significant deterioration is seen during periods 3→4. However, as the ISE generally decreased during the other periods, it is considered that the on-line real-time NLSSQP performed well in the experiments, too, although the the parameter error (Fig. 14(D)) was larger than in the simulation result.

Figure 15 overlaps the time responses during five periods. The response y_r of the reference model is also plotted (broken line). At the $\widetilde{n_e}$ step-up shown in the upper panel of Fig. 15, the

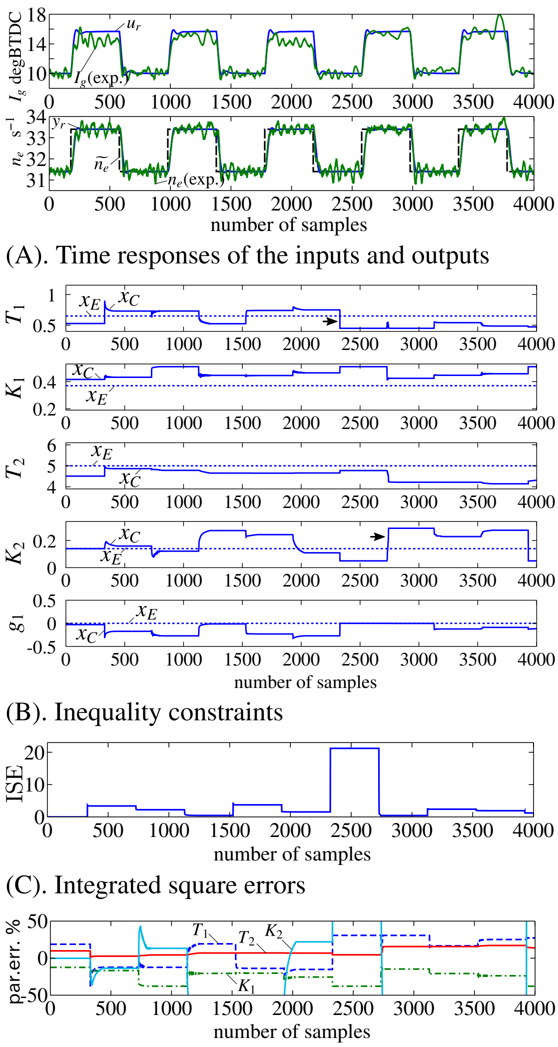

(A). Time responses of the inputs and outputs

(B). Inequality constraints

(C). Integrated square errors

(D). Coincidence ratios of the model parameters

Fig. 14. Results of the physical experimented adaptive control

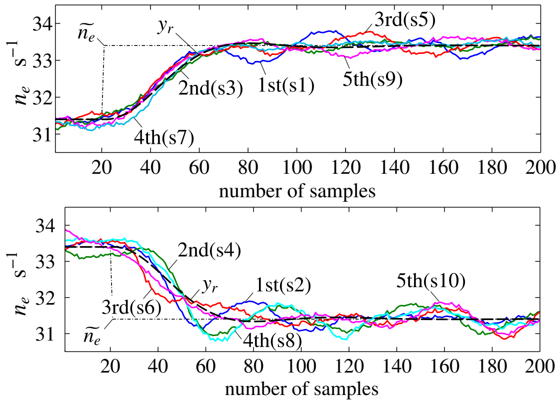

Fig. 15. Comparison between experimental results and the reference y_r

responses y_{p_0}(s1-s9) in each period follow the rise in n_e and well agree with y_r. During the first period, y_{p_0}(s1) slightly deviates from the reference response y_r after the rise, but y_{p_0}(s3-s9) in the later-periods almost correspond to y_r. At the $\widetilde{n_e}$ step-down shown (lower panel of Fig. 15), the n_e fluctuates remarkable, but y_{p_0}(s2-s10) reasonably agree with y_r on average. These results confirm that the adaptation was completed at the second $\widetilde{n_e}$ change and the setting settling time $\widehat{T_s}(2)$=3s was satisfied, as observed in the simulation result.

From these results, we conclude that the developed adaptive control system satisfies the setting settling time in the experiments. Further improvement can be expected by considering the combustion variation.

6. CONCLUSION

This paper investigated a servo system designed to satisfy the setting settling time with small maximum overshoot, and an adaptation method developed through non-linear programming. The designed system was applied to a gasoline engine speed controller and its effectiveness was demonstrated in simulation and experimental tests. The results validated the design method for the model-based adaptive-control system using the model parameters of the controlled object.

REFERENCES

Åström, K. and Hägglund, T. (1995). *PID Controllers:Theory, Design, and Tuning*, ISA.

Ichikawa, K. (1985) Control System Design Based on Exact Model Matching Techniques, *Lecture Notes in Control and Information Sciences, 74*, Springer-Verlag.

Kaneko, O. (2013), Data-Driven Controller Tuning:FRIT approach, *11th IFAC ALCOSP*, 326–336.

Manabe, S. (1998). Coefficient Diagram Method, *IFAC Automatic Control in Aerospace*, 211–222.

Ohta, Y., Takiyama, T, and Masubuchi, I. (2014). Design of Servo Systems to Attain the Given Setting Time(in Japanese). *Trans. of ISCIE*, **27**(1), 1–7.

Takahashi, S., Yamaki, N. and Yabe, H. (1987). Some Modifications of Sequential Quadratic Programming Method for Constrained Optimization, *TRU Mathematics*, Science University of Tokyo, **23**(2), 281–295.

Takiyama, T. (2014). Investigation on the Highly Precise Air Fuel Ratio Adaptive Control in Transient States under Changes in the Intake Valve Opening Timing. *SAE Tech. Paper*,[DOI]10.4271/2014-01-1162.